Anvil cloud thinning implies greater climate sensitivity

Adam B. Sokol[1*], Casey J. Wall[2] and Dennis L. Hartmann[1]

[1]Department of Atmospheric Sciences, University of Washington, Seattle, WA, USA.
[2]Department of Geosciences, University of Oslo, Oslo, Norway.

*Corresponding author(s). E-mail(s): abs66@uw.edu;

Abstract

High clouds produced by tropical convection are expected to shrink in area as climate warms, and the radiative feedback associated with this change has long been the subject of controversy. In a recent assessment of climate sensitivity, the World Climate Research Programme (WCRP) estimated that this feedback is substantially negative, albeit with substantial uncertainty. Here we show that such a negative feedback is not supported by an ensemble of high-resolution atmospheric models. Rather, the models suggest that changes in cloud area and opacity act as a modest positive feedback. The positive opacity component arises from the disproportionate reduction in the area of thick, climate-cooling clouds relative to thin, climate-warming clouds. This suggests that thick cloud area is tightly coupled to the rate of convective overturning—which is expected to slow with warming—whereas thin cloud area is influenced by other, less certain processes. The cloud response is examined from a novel perspective that treats high clouds as part of an optical continuum rather than entities with fixed opacity. The positive feedback differs significantly from previous estimates and leads to a +0.3 °C shift in the median estimate of equilibrium climate sensitivity relative to a previous community assessment.

Keywords: cloud feedback, climate sensitivity, tropical convection

Anvil clouds produced by deep convection are widespread in the Tropics and are a leading source of uncertainty in the recent assessment of climate sensitivity by the WCRP [1]. Thermodynamic arguments predict that anvil cloud area decreases as the surface warms [2, 3], but this could produce a positive, negative, or neutral radiative feedback, since, unlike other cloud types, anvils can have both a positive or negative cloud radiative effect (CRE) at different stages of their life cycle [4, 5]. Deep convective towers and fresh, thick anvils have a high albedo and a strong, negative CRE, while thinner, aged anvils exert a modest, positive CRE [6]. Previous estimates of the anvil area feedback are altogether inconclusive; nevertheless, the maximum likelihood value assessed by the WCRP was substantially negative (-0.2 W/m^2/K, with a Gaussian standard deviation of 0.2 W/m^2/K). Here, we will show that such a negative feedback is not supported by an ensemble of state-of-the-art, cloud-resolving models (CRMs). To the contrary, the models predict that reductions in high cloud area come mostly from thick, reflective anvil clouds that cool the climate. The clouds left behind are optically thinner on average and have a more positive climatological CRE.

Previous work examining the relationship between surface temperature (T_s) and convective cloud area generally supports a reduction in cloud area with warming, albeit with regional and methodological sensitivities [7–17]. Estimates of the associated radiative feedback, however, range from significantly negative [11, 14, 18] to nearly neutral [7] or slightly positive [17, 19–22]. This continued uncertainty may arise, in part, from the use of various cloud classifications (e.g., cirrus, high cloud, anvil, stratiform, etc.) based on arbitrary thresholds that vary from study to study. In reality, tropical convection generates a continuum of ice clouds, with thick cumulonimbi on one end and thin cirrus on the other. This continuum perspective is valuable because it reflects real physical processes—the production, gradual thinning, and eventual dissipation of ice clouds—and provides an intuitive way of understanding the role of convectively generated clouds in tropical climate.

Here, we examine the ice cloud continuum using ice water path (IWP) as a coordinate. IWP—the total mass of condensed ice in the atmospheric column—can be estimated from satellite observations, is easily calculated from model output, and is closely linked to CRE and cloud optical depth (τ; Fig. S1). Changes in the frequency distribution of IWP are therefore informative for understanding the impact of ice clouds on the top-of-atmosphere radiative balance.

We apply the continuum perspective to an ensemble of cloud-resolving models (CRMs) in which deep convection and anvil evolution are explicitly simulated. As part of the Radiative-Convective Equilibrium Model Intercomparison Project (RCEMIP) [23], these models were run on a limited-area, oceanic domain large enough to permit large-scale convective organization (Methods). Simulations were conducted for three fixed, uniform T_s values (295, 300, and 305 K). We will show that the ice cloud response to warming is characterized by two regimes: a robust reduction in thick ice cloud area that is

consistent with existing thermodynamic arguments, and a small but uncertain change in thin ice cloud area. Such changes produce an overall thinning of the cloud population and a positive opacity feedback, implying a +0.3 °C shift in the WCRP estimate of equilibrium climate sensitivity.

Results

Convective clouds as a continuum of ice

The continuum of tropical ice clouds can be represented by a discrete frequency distribution of IWP [24, 25]. We denote this distribution as f(IWP), which can be interpreted as the IWP-resolved cloud fraction. Similarly, we denote the mean CRE of convectively generated ice clouds as CRE(IWP) (Methods). Satellite-derived estimates of f from the tropical West Pacific, along with model-estimated CRE, provide an intuitive understanding of convective cloud evolution (Fig. 1). At high IWP ($> 10^3$ g/m^{-2}), deep convective cores have a large, negative CRE but cover a small area. As IWP decreases, f and CRE both increase rapidly, which reflects the thinning and spreading of detrained anvils. Maximum f occurs around 15-35 g/m^2 (τ ~1-2; Supplementary Fig. 1), which approximately coincides with the maximum CRE; the most abundant anvil clouds are therefore those with the strongest warming effect. These clouds counteract the cooling effect of thicker clouds, leading to a climatological CRE near zero in tropical convective regions [26, 27].

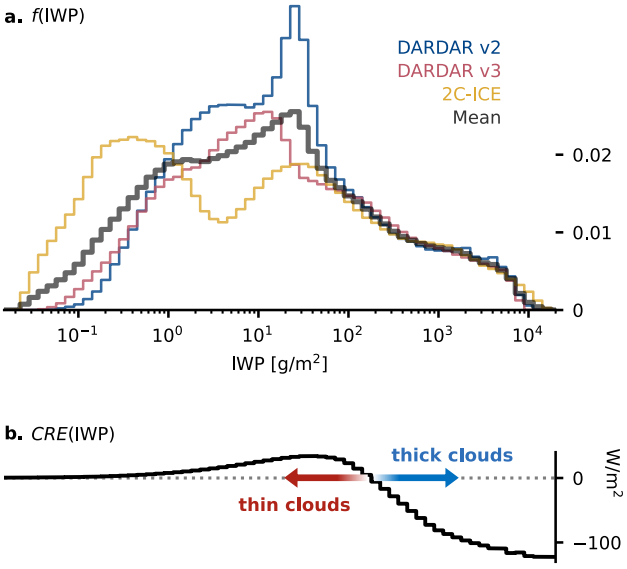

Fig. 1 The tropical ice cloud continuum. **(a)** f(IWP) derived from satellite observations of the tropical West Pacific (150-180°E, 15°S-15°N) for 2009. Three satellite retrievals and their mean are shown (Methods). **(b)** Multimodel mean CRE(IWP) for the CRM simulations with T_s=300 K. Low cloud effects are treated as described in Methods.

The CRM ensemble produces a wide variety of IWP distributions with varying degrees of similarity to the satellite-derived f (Fig. 2). Several aspects of the observed distribution are well reproduced by the models: the maximum IWP of 2-4$\times 10^4$ g/m^2, the inflection point around 10^3 g/m^2, and the rapid increase in f as IWP decreases from there. Most of the models are therefore capturing the basic thinning and spreading of anvil clouds after detrainment. Their performance is more mixed when it comes to the observed maximum at 15-35 g/m^2, with about half producing a relative maximum or plateau within the observed range. That half of the models place the peak within the narrow IWP range constrained by observations suggests that the physical processes responsible for the maximum can be captured even in idealized representations of the tropical atmosphere.

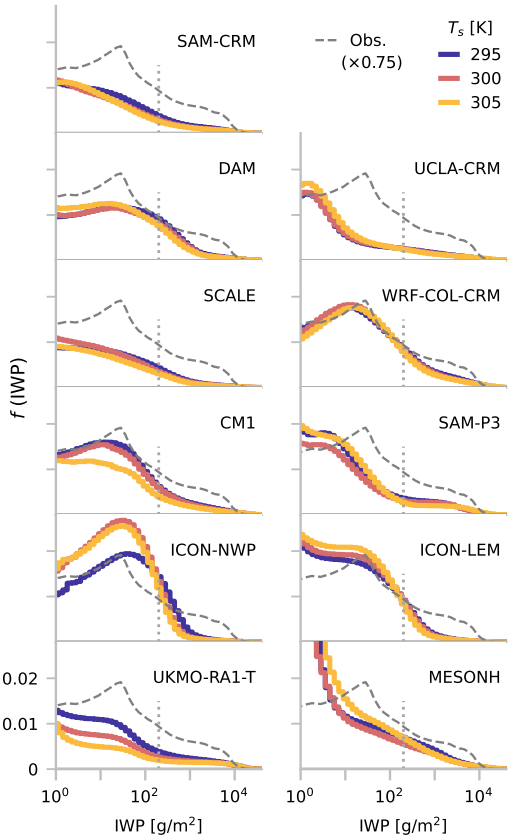

Fig. 2 Model representations of the ice cloud continuum. Panels show the IWP distributions f(IWP) for each model and each T_s. Dashed grey lines show the mean of the three satellite-derived estimates of f, scaled arbitrarily by a factor of 0.75 to aid comparison of distribution shapes. Vertical, dotted grey lines mark the cutoff between thick and thin clouds.

In the deep Tropics, the ice cloud continuum is dominated by clouds with tops near the level of deep convective detrainment [28]. Mid-level ice clouds are very rare in the observations and model simulations considered here (Supplementary Figs. 2-3), so we are confident that f reflects a continuum of high clouds consisting of deep convective towers, their attached anvils, and thin cirrus of convective or in-situ origin (Supplementary Fig. 4). Based on Fig. 1, the continuum can be divided into two categories with physical relevance for cloud-climate interactions: clouds with $CRE < 0$ and those with $CRE > 0$. We refer to these as thick and thin clouds, respectively, and separate them by an IWP threshold corresponding to the change in sign of the multimodel mean CRE. The area fractions covered by thick and thin clouds are then

$$f_{\text{thick}} = \sum_{200\,\text{g/m}^2}^{\infty} f$$

$$f_{\text{thin}} = \sum_{1\,\text{g/m}^2}^{200} f$$

and the total ice cloud fraction is $f_{\text{ice}} = f_{\text{thick}} + f_{\text{thin}}$. Clouds with IWP<1 g/m^2 have a small CRE and are excluded from our analysis, which does not affect our results (Supplementary Discussion 1).

The domain-averaged CRE of ice clouds, denoted here as C_{ice}, can be similarly decomposed into thick- and thin-cloud contributions, C_{thick} and C_{thin}, respectively. We first define the area-weighted CRE as

$$C(\text{IWP}) = f \cdot CRE \tag{1}$$

which represents the CRE of a particular IWP bin averaged over the entire domain. Then, as with f, C_{ice}, C_{thick}, and C_{thin} are found by summing C over the relevant IWP intervals (Methods; Supplementary Fig. 5).

Ice cloud thinning in response to warming

The response of f to surface warming varies substantially across the ensemble (Fig. 2a, Supplementary Figs. 6-7). To identify robust aspects of the response, we compute the multimodel mean fractional change in f between 295–305 K (Fig. 3a). This shows that f increases with warming at the largest IWPs, reflecting an increase in the ice content of the strongest convective updrafts. Otherwise, we find that thick clouds consistently contract across the entire ensemble, with a mean change in f_{thick} of -2 %/K. This change, reflective of a decrease in the area occupied by deep convective cores and fresh anvils, is in line with the anticipated weakening of the mean convective mass flux [29–31]. In theory, this weakening could manifest as a decrease in the convective area fraction, a decrease in the vertical velocity within convection, or some combination thereof. Since convective storms are expected to be *more*

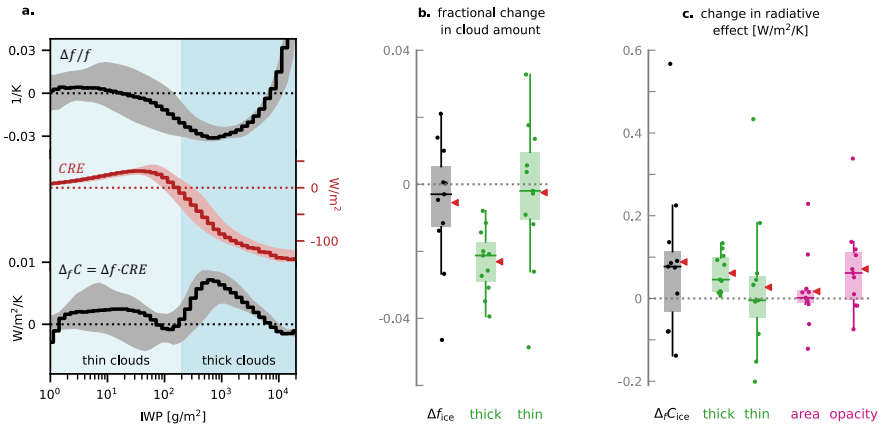

Fig. 3 The ice cloud response to warming and its radiative effects. (a) fractional change in f(IWP), CRE(IWP) for $T_s = 295$ K, and $\Delta_f C$, the change in domain-averaged CRE due to changes in f alone. Lines show multimodel means and shading shows 25-75th percentiles. **(b)** Fractional change in f_{ice} and its decomposition into thick- and thin-cloud components. **(c)** the combined area and opacity feedback $\Delta_f C_{\text{ice}}$, its thick- and thin-cloud components, and its area and opacity components. All changes are evaluated between 295 and 305 K and normalized by ΔT_s. For box plots, boxes show Q1-Q3 and outliers differ from Q1 or Q3 by at least 1.5xIQR. Dashes show medians, red triangles show means, and dots show individual models.

vigorous with warming [32, 33], it seems likely that convective area fraction decreases. This could arise from a reduction in the number of convective events or a decrease in their typical width, but the present analysis does not discern between these two mechanisms. Regardless, the reduction in f_{thick} seen here suggests that changes in convective area fraction affect not only deep convective cores, but also fresh, thick anvil clouds, which are typically attached to convective cores and undergo relatively rapid thinning after their formation [34, 35]. The impressive agreement between the CRMs (Fig. 3b, Supplementary Fig. 6c) suggests that this response is rooted in fundamental physics shared by all of the models.

In contrast to the reduction in f_{thick}, there is no model consensus on changes in thin cloud area. The ensemble is evenly split on the sign of Δf_{thin}, resulting in a small ensemble mean response despite wide intermodel spread (Fig. 3b). The mismatch between changes in f_{thick} and f_{thin} suggests that the thin cloud response is not as tightly constrained by changes in the convective mass flux. This is in line with our current understanding that the spreading, thinning, and maintenance of aged anvils are driven by various microphysical and radiative processes that are not directly related to the total convective mass flux [4, 5, 36–38]. Intermodel differences in the representation of these processes (particularly microphysics) almost certainly impact the simulated thin cloud response. With these insights into the anvil life cycle, it is perhaps unsurprising that Δf_{thin} is poorly constrained compared to Δf_{thick}. Since thin clouds are much more abundant than thick ones (Supplementary

Table 1), changes in f_{ice} largely reflect those in f_{thin} (Supplementary Table 2). Intermodel spread in Δf_{ice} is best explained by Δf at ∼20 g/m^2 (r^2=0.92; Supplementary Fig. 8), which closely corresponds to the most abundant IWP in observations and some models.

With a robust reduction in f_{thick} and a small mean change in f_{thin}, the ensemble suggests that the ice cloud population becomes thinner in response to surface warming. The ratio of thin to thick clouds increases in all but one of the models (Supplementary Fig. 7), demonstrating that this thinning can occur regardless of whether f_{ice} increases, decreases, or stays the same. The thinning is qualitatively consistent with recent observational and model-based analyses [8, 16, 21, 39, 40].

A positive opacity feedback

We now seek to understand how changes in the ice cloud continuum affect C_{ice}, the domain-averaged CRE of ice clouds. The change in C due solely to changes in f is expressed as

$$\Delta_f C(\text{IWP}) = CRE \cdot \Delta f \tag{2}$$

where Δ_f denotes the change due to f alone, normalized by ΔT_s, and CRE is evaluated at the initial T_s. As before, $\Delta_f C_{\text{thick}}$, $\Delta_f C_{\text{thin}}$, and $\Delta_f C_{\text{ice}}$ are found by summing $\Delta_f C$ over the respective IWP intervals. $\Delta_f C_{\text{ice}}$ can be interpreted as a combined area and opacity feedback, although it neglects the part of the opacity feedback related to changes in cloud microphysics (Methods).

We assess $\Delta_f C$ and $\Delta_f C_{\text{ice}}$ separately for each model between 295–305 K. All but three produce positive $\Delta_f C_{\text{ice}}$ (Fig. 3c), demonstrating that cloud thinning can lead to an increase in climatological CRE regardless of whether f_{ice} increases or decreases. The ensemble mean $\Delta_f C_{\text{ice}}$ is +0.09 W/m^2/K; nearly all of this increase comes from thick cloud changes, while the mean thin-cloud contribution is again very small but with considerably more spread (Fig. 3, Supplementary Fig. 6d). Intermodel spread in $\Delta_f C_{\text{ice}}$ is well explained by its thin-cloud component (r^2=0.95) and best predicted by $\Delta_f C$ at 40-70 g/m^2 (r^2=0.97; Supplementary Fig. 8).

$\Delta_f C_{\text{ice}}$ can be decomposed into two parts analogous to conventional cloud area and opacity feedbacks (Methods). The area component assumes a uniform fractional change in f and no change in $\overline{CRE}$, the conditionally averaged CRE of ice clouds. In most of the models, the area component is very small (Fig. 3c), either because Δf_{ice} is small or because the ice cloud population is about radiatively neutral to begin with. This is in line with previous arguments suggesting that the radiative neutrality of convective clouds constrains the area feedback to be small [41].

The opacity component of $\Delta_f C_{\text{ice}}$ accounts for changes in $\overline{CRE}$ brought about by nonuniform changes in f, such as the thinning of the cloud population described above. Unlike the area component, the opacity component is generally positive across the ensemble (Fig. 3c), reflecting a mean increase in $\overline{CRE}$

due to cloud thinning. The multimodel-mean opacity component accounts for nearly all of the magnitude of $\Delta_f C_{\text{ice}}$, suggesting that when it comes to anvil radiative feedbacks, shifts in opacity are more important than changes in total area. The CRMs show impressive agreement in this regard, as does at least one general circulation model with parameterized convection [21]. Again, inter-model spread in the area and opacity components is well explained by the spread in Δf_{thin} (Supplementary Fig. 9).

Implications for climate sensitivity

The positive anvil area and opacity feedback predicted by the CRM ensemble represents a significant departure from the WCRP estimate (Supplementary Discussion 2) and suggests that clouds act to enhance global warming more than is assumed in the WCRP assessment of equilibrium climate sensitivity (ECS). To update that assessment, we replace the previous feedback estimate with our RCEMIP-informed value and generate a new probability density function (PDF) of ECS. We calculate the RCEMIP-informed value by converting the multimodel mean $\Delta_f C_{\text{ice}}$ to a global mean feedback (Methods). This gives a feedback estimate of $N(0.03, 0.06)$ W/m^2/K, where, following the WCRP convention [1], $N(x, y)$ is a Gaussian with mean x and standard deviation y, which we set equal to the feedback standard deviation across the RCEMIP ensemble. While the RCEMIP-informed feedback is small in magnitude compared to other cloud feedbacks, it is a large change from the previous estimate and corresponds to a 51% increase in the WCRP-assessed total cloud feedback.

Updating the feedback results in a broad +0.3 °C shift in the ECS PDF (Fig. 4). The central estimate (median) increases from 3.1 to 3.4 °C, and the 66% likely range from 2.6-3.9 to 2.8-4.2 °C (Supplementary Table 3). The ∼10% widening of the likely range is counterintuitive given the reduction in anvil feedback uncertainty relative to the WCRP assessment. The reduction in uncertainty is outweighed by the increase in the central estimate of the feedback, which acts to broaden the PDF due to the nonlinear relationship between ECS and feedback strength [42]. The likelihoods of extreme ECS values are most dramatically affected by the feedback update: the probability of ECS>6 °C doubles, while that of ECS<2 °C is reduced by 74%. Sensitivity tests (Methods) show that the shift in the PDF results from the increase in the central estimate of the feedback and is quite insensitive to the feedback uncertainty (Supplementary Fig. 10, Supplementary Table 3).

Extrapolating from RCEMIP to a global mean feedback comes with the caveat that certain atmospheric changes cannot be captured in such idealized simulation setups. For example, our feedback estimate cannot account for warming-induced changes in planetary-scale circulation or dynamical modes of variability, which could affect patterns of convection and cloudiness. However, the RCEMIP CRMs produce a wide range of changes in large-scale convective organization in response to warming [43]; these changes freely affect cloud properties and are thus implicitly included in our analysis. We are therefore confident that our estimate spans a wide range of possible changes in large-scale

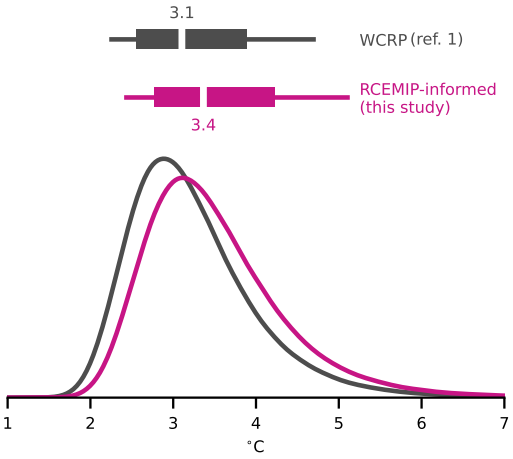

Fig. 4 Updating the probability density function of ECS. Grey: WCRP baseline estimate from [1], which uses an anvil area feedback of $N(-0.20, 0.20)$ W/m^2/K, where $N(x, y)$ is a Gaussian with mean x and standard deviation y. Pink: updated calculation using the RCEMIP-informed value of $N(0.03, 0.06)$ W/m^2/K. Above, the thin horizontal lines and boxes show 90% and 66% confidence intervals, respectively, and white dashes show the central estimate (median).

convective dynamics. Furthermore, we have already shown that the CRMs capture the expected reduction in deep convective area in response to warming; this, along with previous work showing that the ensemble-predicted changes in cloud altitude and temperature are consistent with observational and theoretical expectations [43, 44], adds confidence that the most fundamental aspects of the convective response are well represented by the CRMs.

Discussion

A main takeaway of this work is that changes in tropical ice cloud opacity are a critical part of the cloud response to warming. The possibility of a high cloud opacity feedback has been noted before [18, 21, 45] but has received comparatively little attention in broader discussions of cloud feedback and ECS. Previous assessments have often assumed fixed anvil opacity [11, 20], perhaps due to the lack of *a priori* expectations for how changes in area would be spread across the distribution of clouds observed in the present-day Tropics. By treating tropical ice clouds as a continuum, this work provides an initial characterization of that response. While our estimate of the combined area and opacity feedback is small, it constitutes a significant increase from the WCRP estimate [1] and implies a substantial shift in the PDF of ECS.

The continuum framework has revealed that thick, climate-cooling and thin, climate-warming clouds are affected differently by changes in T_s. The robust decrease in thick cloud area mirrors expected changes in convective mass flux, whereas the uncertain thin-cloud response appears to be influenced by

other factors. In particular, thin clouds with IWP between 20-70 g/m^2 (τ ~1-3) are the leading source of uncertainty in changes in ice cloud area and radiative effect. These clouds are known to be shaped by various radiative, dynamic, and microphysical processes that may respond to warming in complex ways [46]. Constraining these changes is a challenging undertaking that requires consideration of a wide range of physical scales, but such an endeavor may prove critical for understanding tropical climate change.

Acknowledgments. We thank three anonymous reviewers for their helpful feedback, Catherine Stauffer for processing and sharing RCEMIP data, Lily Hahn for helpful feedback on this manuscript, and Jakob Deutloff for helpful conversations about the treatment of cloud overlap. We acknowledge the many scientists who provided simulations for RCEMIP and the German Climate Computing Center (DKRZ) for hosting the standardized RCEMIP data. This work was supported by NASA FINESST grant 80NSSC20K1613 and NSF grant AGS-2124496.

Supplementary information. Supplementary Discussions 1-2, Figures 1-13, and Tables 1-3.

Methods

Satellite Observations of IWP

The three satellite retrievals shown in Fig. 1b are combined radar-lidar retrievals that use measurements from the CALIOP lidar [47] and the CloudSat radar [48]. Both instruments are part of the A-train satellite constellation. The three retrievals are DARDAR-Cloud version 2.1.1 [49], DARDAR-Cloud version 3.1 [50], and 2C-ICE R05 [51]. The two versions of DARDAR-Cloud differ principally in their treatment of cloudy volumes detected by the lidar only [50].

Cloud-resolving model ensemble

We use output from the "RCE_large" simulations of RCEMIP. The full simulation protocol is described in [23]. Briefly, the simulations have a domain size of ~6,000×400 km^2 with 3-km horizontal resolution. They used three fixed, uniform sea surface temperatures (295, 300, and 305 K) and were integrated for 100 days. We use the instantaneous 3D output (every 6 hours) from the last 25 days of each run. Instantaneous IWP is computed by vertically integrating the total (precipitating and nonprecipitating) atmospheric ice content. We included precipitating ice to be consistent with the satellite observations, which do not distinguish between ice types.

Our analysis includes all of the RCEMIP CRMs for which the necessary, standardized output is publicly available, with the exception of UKMO-RA1-T-nocloud and UKMO-CASIM. UKMO-RA1-T-nocloud is the same as UKMO-RA1-T apart from its deactivation of a subgrid cloud scheme.

UKMO-CASIM is excluded because the unique vertical structure of convection in that model produces an IWP distribution that does not reflect deep convective cloud climatology, but rather expansive, stratiform ice clouds produced by convective detrainment near the freezing level. We also include the RCEMIP_large-style simulations described in [52], which use the SAM model [53] with P3 microphysics [54] (referred to as SAM-P3).

Calculation of *CRE*(IWP) and treatment of low clouds

For each column of model output, CRE is computed as the difference between hourly mean all-sky and clear-sky radiative fluxes. We seek to calculate $CRE(\text{IWP})$ such that it reflects the radiative effects of clouds produced by deep convection while excluding the effects of unrelated liquid clouds below. To this end, we first compute the mean CRE of all columns falling within each IWP bin (the "all-cloud" CRE) as well as that of the columns with liquid water path below 1 g/m^2 (the "ice-only" CRE). Liquid clouds found in low-IWP columns are typically low clouds at the top of the boundary layer, which are unrelated to the overlying ice clouds but nevertheless have an impact on the top-of-atmosphere CRE [55]. Therefore, to exclude their radiative effects from $CRE(\text{IWP})$, we set $CRE(\text{IWP})$ equal to the ice-only for IWP $< 10^2$ g/m^2. On the other hand, liquid found in high-IWP columns is typically part of same deep convective cloud as the ice above; we seek to include these liquid effects and therefore set $CRE(\text{IWP})$ equal to the all-sky CRE for IWP $> 10^3$ g/m^2. Between 10^2 and 10^3 g/m^2, we use a transition that is linear with respect to $\log_{10}$IWP (Supplementary Fig. 11). These thresholds were selected based on the multimodel mean liquid cloud fraction within each IWP bin (Supplementary Fig. 12), which increases rapidly between inflection points at 10^2 and 10^3 g/m^2, signaling a shift from low clouds unrelated to the high clouds above to deep convective clouds occupying a large portion of the atmospheric column. Our results are not sensitive to the details of this transition, and the multimodel mean $CRE(\text{IWP})$ for T_s=295 K changes sign at ∼200 g/m^2 (τ ∼4-5; Supplementary Fig. 1) , which is consistent with previous analyses [24, 56, 57].

Definitions in the IWP framework

We have defined $f(\text{IWP})$ and $CRE(\text{IWP})$ as the IWP-resolved cloud fraction and CRE, respectively. We have also defined the area-weighted CRE as $C(\text{IWP}) = f(\text{IWP}) \cdot CRE(\text{IWP})$. For any parameter $X(\text{IWP})$, we compute the thick and thin cloud contributions to the domain mean as

$$X_{\text{thick}} = \sum_{200\,\text{g/m}^2}^{\infty} X$$

$$X_{\text{thin}} = \sum_{1\,\text{g/m}^2}^{200} X$$

and the total ice cloud contribution as $X_{\text{ice}} = X_{\text{thick}} + X_{\text{thin}}$. This notation is applied to $f(\text{IWP})$ and $C(\text{IWP})$ throughout the paper, with f_{ice} and C_{ice} thus representing the domain-averaged ice cloud fraction and the domain-averaged ice cloud radiative effect, respectively. The conditionally averaged ice cloud CRE is defined as $\overline{CRE} = C_{\text{ice}}/f_{\text{ice}}$.

Analytical expressions for cloud feedback in the IWP Framework

The Cess-type cloud feedback is defined as the change in domain-averaged CRE normalized by ΔT_s [58]. It differs slightly from the formal cloud feedback parameter computed by partial radiative perturbation [59]. In traditional feedback analysis, the total cloud feedback is often decomposed into cloud altitude, area, and opacity components. Resolved across the IWP continuum, the total Cess-type, ice cloud feedback is expressed as

$$\Delta C(\text{IWP}) = CRE \cdot \Delta f + f \cdot \Delta CRE + \Delta f \cdot \Delta CRE \tag{3}$$

where all variables are functions of IWP and all Δ terms are assumed to be normalized by ΔT_s. The final term on the right-hand side is a small nonlinear term that we neglect here. The second term on the right-hand side accounts for changes in $CRE(\text{IWP})$, which may occur due to changes in clear-sky fluxes or cloud temperature, altitude, and microphysical structure. This term encompasses so-called cloud masking effects [59], the entire ice cloud altitude feedback, as well as the microphysical part of the opacity feedback, which manifests as a change in the optical depth associated with a particular IWP. While this term is significant (Supplementary Fig. 13), it is not our focus here.

The first term on the right-hand side of Eq. 2, which we define as $\Delta_f C$, is the part of ΔC attributable to changes in the frequency of a particular IWP. $\Delta_f C_{\text{ice}}$, equal to the sum of $\Delta_f C$ across all IWP > 1 g/m^2, is thus the change in the domain-averaged CRE of ice clouds due to changes in f alone. $\Delta_f C_{\text{ice}}$ encompasses the entire ice cloud area feedback and the remaining part of the ice cloud opacity feedback, since nonuniform changes in f can drive changes in mean ice cloud opacity. To formally separate the area and opacity components, we first define the fractional change in $f(\text{IWP})$ as

$$g(\text{IWP}) = \frac{\Delta f}{f} \tag{4}$$

which can be decomposed as

$$g(\text{IWP}) = G + g'(\text{IWP}) \tag{5}$$

where $G = \Delta f_{\text{ice}}/f_{\text{ice}}$ is the fractional change in total ice cloud fraction and g' is the deviation from G at a particular IWP. Combining equations (4) and (5) yields

$$\Delta f = f \cdot (G + g') \tag{6}$$

which when substituted into equation (2) yields

$$\Delta_f C = C(G + g') \tag{7}$$

where we have employed equation (1). $\Delta_f C_{\text{ice}}$ is then found by summing over all IWP > 1 g/m^2:

$$\Delta_f C_{\text{ice}} = G \sum_{1\,\text{g/m}^2}^{\infty} C + \sum_{1\,\text{g/m}^2}^{\infty} g' C \tag{8}$$

which, using the definitions of C_{ice} and G, simplifies to

$$\Delta_f C_{\text{ice}} = \Delta f_{\text{ice}} \cdot \overline{CRE} + \sum_{1\,\text{g/m}^2}^{\infty} g' C \tag{9}$$

The first term on the right-hand side is the area component of $\Delta_f C_{\text{ice}}$, which is attributable to changes in total ice cloud fraction assuming fixed $\overline{CRE}$ (i.e., a uniform fractional change in f across all IWP). The second term is the opacity component, which accounts for deviations from a uniform fractional change, which causes bulk thinning or thickening of the ice cloud population and may affect $\overline{CRE}$. The opacity component does not account for the microphysically driven opacity changes included in the second term of Eq. 3.

Recently, [17] developed a simplified expression for the anvil cloud area feedback (their Equation 9, which they refer to as the Iris feedback). Unlike the Cess-type feedbacks discussed above, their expression aligns with traditional feedback formalism. Discretizing their expression shows that it is the same as the cloud area component of equation (9), with the addition of a cloud overlap term. Therefore, $\Delta_f C_{\text{ice}}$ can be interpreted as the sum of the ice cloud area feedback and the part of the opacity feedback related to changes in f. With regard to our treatment of cloud overlap here, the formulation of CRE(IWP) described above must be kept in mind. Whether or not the radiative effects of cloud liquid are included in $\Delta_f C$ depends on IWP. At high IWPs corresponding to deep convective cores and very thick anvil clouds, we have assumed that any liquid present in the column belongs to the same cloud system as the ice, and the all-sky CRE is thus used to evaluate $\Delta_f C$. On the other hand, at low IWPs, $\Delta_f C$ is evaluated using the ice-only CRE. This means, for example, that the ice-free area exposed by a reduction in f is partially occupied by low clouds exerting a negative radiative effect. The low-cloud CRE in the newly exposed regions is assumed to be equal to the difference between the all-sky and ice-only CREs. This is likely an underestimate, since the CREs of overlapping low and high clouds are not simply additive in reality. However, the impact of this bias on $\Delta_f C_{\text{ice}}$ is small due to compensating effects of

models with increasing and decreasing thin cloud area. To account for this potential uncertainty, our analysis of equilibrium climate sensitivity (ECS) includes sensitivity tests, described below.

Converting $\Delta_f C_{\text{ice}}$ to a global mean feedback and estimating ECS

The ensemble mean $\Delta_f C_{\text{ice}}$ represents the anvil cloud area and opacity feedback, which we take to be valid over Earth's tropical oceans. To convert this to a global mean feedback, we multiply by the fractional area of the tropical oceans (37%) and assume that the Tropics warm by 0.9 °C for every degree of global mean warming [60]. This results in the reported feedback value of $N(0.03, 0.06)$ W/m^2/K, where the Gaussian standard deviation is set equal to the standard deviation of the feedback across the RCEMIP ensemble. We then generated updated probability density function of ECS using the Bayesian inference code from [1] with all three lines of evidence used in their original analysis (historical, process-based, and paleoclimatological).

We conduct sensitivity tests to account for additional sources of uncertainty that may not be captured by the standard deviation of the RCEMIP ensemble. For example, changes in cloud microphysical structure could contribute to the opacity feedback but are not included in our estimate due to model output limitations. Overlap between high and low clouds, some of which is accounted for in our estimate, is another possible source of model bias and feedback uncertainty. To assess the impact of greater feedback uncertainty, we run the ECS calculations for additional feedback values of $N(0.03, 0.16)$ and $N(0.03, 0.20)$ W/m^2/K. The value of 0.16 W/m^2/K is the maximum deviation of any individual model from the multimodel mean and thus encompasses the full ensemble spread. The value of 0.20 W/m^2/K is the WCRP-assessed uncertainty from [1], intended to serve as an upper bound. As shown in Supplementary Fig. 10 and Supplementary Table 3, the resulting PDFs are very similar to that for $N(0.03, 0.06)$.

Data availability. The DARDAR-Cloud satellite products are available at https://www.icare.univ-lille.fr/dardar/data-access/ and the 2C-ICE products at https://www.cloudsat.cira.colostate.edu/data-products/2c-ice. RCEMIP model output is publicly available at http://hdl.handle.net/21.14101/d4beee8e-6996-453e-bbd1-ff53b6874c0e, and full output from the SAM-P3 model runs is available from the corresponding author on request. The derived data needed to reproduce the figures in this paper is available at https://github.com/adambsokol/Ice-cloud-feedbacks-in-RCEMIP.

Code availability. The code used for the climate sensitivity calculations is available from ref. 1 at https://zenodo.org/record/3945276#.ZFvtAOzMJ8Z. Upon publication, the code needed to generate the figures in this paper will be added to the repository at https://github.com/adambsokol/Ice-cloud-feedbacks-in-RCEMIP.

References

[1] Sherwood, S. C. *et al.* An Assessment of Earth's Climate Sensitivity Using Multiple Lines of Evidence. *Reviews of Geophysics* **58** (4) (2020). https://doi.org/10.1029/2019RG000678 .

[2] Zelinka, M. D. & Hartmann, D. L. Why is longwave cloud feedback positive? *Journal of Geophysical Research Atmospheres* **115** (16) (2010). https://doi.org/10.1029/2010JD013817 .

[3] Bony, S. *et al.* Thermodynamic control of anvil cloud amount. *Proceedings of the National Academy of Sciences* **113** (32), 8927–8932 (2016). https://doi.org/10.1073/pnas.1601472113 .

[4] Hartmann, D. L., Gasparini, B., Berry, S. E. & Blossey, P. N. The Life Cycle and Net Radiative Effect of Tropical Anvil Clouds. *Journal of Advances in Modeling Earth Systems* **10** (12), 3012–3029 (2018). https://doi.org/10.1029/2018MS001484 .

[5] Gasparini, B., Blossey, P. N., Hartmann, D. L., Lin, G. & Fan, J. What Drives the Life Cycle of Tropical Anvil Clouds? *Journal of Advances in Modeling Earth Systems* **11** (8), 2586–2605 (2019). https://doi.org/10.1029/2019MS001736 .

[6] Hartmann, D. L. & Berry, S. E. The balanced radiative effect of tropical anvil clouds. *Journal of Geophysical Research* **122** (9), 5003–5020 (2017). https://doi.org/10.1002/2017JD026460 .

[7] Ito, M. & Masunaga, H. Process-Level Assessment of the Iris Effect Over Tropical Oceans. *Geophysical Research Letters* **49** (7), e2022GL097997 (2022). https://doi.org/10.1029/2022GL097997 .

[8] Kubar, T. L. & Jiang, J. H. Net Cloud Thinning, Low-Level Cloud Diminishment, and Hadley Circulation Weakening of Precipitating Clouds with Tropical West Pacific SST Using MISR and Other Satellite and Reanalysis Data. *Remote Sensing* **11** (10), 1250 (2019). https://doi.org/10.3390/rs11101250 .

[9] Saint-Lu, M., Bony, S. & Dufresne, J.-L. Observational Evidence for a Stability Iris Effect in the Tropics. *Geophysical Research Letters* **47** (14) (2020). https://doi.org/10.1029/2020GL089059 .

[10] Saint-Lu, M., Bony, S. & Dufresne, J.-L. Clear-sky control of anvils in response to increased CO2 or surface warming or volcanic eruptions. *npj Climate and Atmospheric Science* **5** (1), 1–8 (2022). https://doi.org/10.1038/s41612-022-00304-z .

[11] Lindzen, R. S., Chou, M. D. & Hou, A. Y. Does the Earth Have an Adaptive Infrared Iris? *Bulletin of the American Meteorological Society* **82** (3) (2001). https://doi.org/10.1175/1520-0477(2001)082⟨0417:DTEHAA⟩2.3.CO;2 .

[12] Su, H. *et al.* Variations of tropical upper tropospheric clouds with sea surface temperature and implications for radiative effects. *Journal of Geophysical Research: Atmospheres* **113** (D10) (2008). https://doi.org/10.1029/2007JD009624 .

[13] Zelinka, M. D. & Hartmann, D. L. The observed sensitivity of high clouds to mean surface temperature anomalies in the tropics. *Journal of Geophysical Research: Atmospheres* **116** (D23) (2011). https://doi.org/10.1029/2011JD016459 .

[14] Choi, Y.-S. *et al.* Revisiting the iris effect of tropical cirrus clouds with TRMM and A-Train satellite data. *Journal of Geophysical Research: Atmospheres* **122** (11), 5917–5931 (2017). https://doi.org/10.1002/2016JD025827 .

[15] Igel, M. R., Drager, A. J. & van den Heever, S. C. A CloudSat cloud object partitioning technique and assessment and integration of deep convective anvil sensitivities to sea surface temperature. *Journal of Geophysical Research: Atmospheres* **119** (17), 10515–10535 (2014). https://doi.org/10.1002/2014JD021717 .

[16] Liu, R. *et al.* High cloud variations with surface temperature from 2002 to 2015: Contributions to atmospheric radiative cooling rate and precipitation changes. *Journal of Geophysical Research: Atmospheres* **122** (10), 5457–5471 (2017). https://doi.org/10.1002/2016JD026303 .

[17] McKim, B., Bony, S. & Dufresne, J.-L. Physical and observational constraints on the anvil cloud feedback. Preprint at https://www.authorea.com/users/538471/articles/627002-physical-and-observational-constraints-on-the-anvil-cloud-area-feedback (2023).

[18] Mauritsen, T. & Stevens, B. Missing iris effect as a possible cause of muted hydrological change and high climate sensitivity in models. *Nature Geoscience* **8** (5), 346–351 (2015). https://doi.org/10.1038/ngeo2414.

[19] Chambers, L. H., Lin, B. & Young, D. F. Examination of New CERES Data for Evidence of Tropical Iris Feedback. *Journal of Climate* **15** (24), 3719–3726 (2002). https://doi.org/10.1175/1520-0442(2002)015⟨3719:EONCDF⟩2.0.CO;2 .

[20] Lin, B., Wielicki, B. A., Chambers, L. H., Hu, Y. & Xu, K.-M. The Iris Hypothesis: A Negative or Positive Cloud Feedback? *Journal of Climate* **15** (1), 3–7 (2002). URL https://journals.ametsoc.org/view/journals/clim/15/1/1520-0442_2002_015_0003_tihano_2.0.co_2.xml. https://doi.org/10.1175/1520-0442(2002)015⟨0003:TIHANO⟩2.0.CO;2, publisher: American Meteorological Society Section: Journal of Climate .

[21] Li, R. L., Storelvmo, T., Fedorov, A. V. & Choi, Y.-S. A Positive Iris Feedback: Insights from Climate Simulations with Temperature-Sensitive Cloud–Rain Conversion. *Journal of Climate* **32** (16), 5305–5324 (2019). URL http://journals.ametsoc.org/doi/10.1175/JCLI-D-18-0845.1. https://doi.org/10.1175/JCLI-D-18-0845.1, publisher: American Meteorological Society .

[22] Williams, I. N. & Pierrehumbert, R. T. Observational evidence against strongly stabilizing tropical cloud feedbacks. *Geophysical Research Letters* **44** (3), 1503–1510 (2017). https://doi.org/10.1002/2016GL072202 .

[23] Wing, A. A. *et al.* Radiative–convective equilibrium model intercomparison project. *Geoscientific Model Development* **11** (2), 793–813 (2018). https://doi.org/10.5194/gmd-11-793-2018 .

[24] Berry, E. & Mace, G. G. Cloud properties and radiative effects of the Asian summer monsoon derived from A-Train data. *Journal of Geophysical Research* **119** (15), 9492–9508 (2014). https://doi.org/10.1002/2014JD021458 .

[25] Chen, Y.-W. *et al.* High Cloud Responses to Global Warming Simulated by Two Different Cloud Microphysics Schemes Implemented in the Nonhydrostatic Icosahedral Atmospheric Model (NICAM). *Journal of Climate* **29** (16), 5949–5964 (2016). https://doi.org/10.1175/JCLI-D-15-0668.1 .

[26] Ramanathan, V. *et al.* Cloud-radiative forcing and climate: Results from the earth radiation budget experiment. *Science* **243** (4887), 57–63 (1989). https://doi.org/10.1126/science.243.4887.57 .

[27] Hartmann, D. L., Moy, L. A. & Fu, Q. Tropical Convection and the Energy Balance at the Top of the Atmosphere. *Journal of Climate* **14** (24), 4495–4511 (2001). https://doi.org/10.1175/1520-0442(2001)014⟨4495:TCATEB⟩2.0.CO;2, publisher: American Meteorological Society Section: Journal of Climate .

[28] Stephens, G. *et al.* CloudSat and CALIPSO within the A-Train: Ten Years of Actively Observing the Earth System. *Bulletin of the American Meteorological Society* **99** (3), 569–581 (2018). https://doi.org/10.1175/BAMS-D-16-0324.1 .

[29] Knutson, T. R. & Manabe, S. Time-Mean Response over the Tropical Pacific to Increased C02 in a Coupled Ocean-Atmosphere Model. *Journal of Climate* **8** (9), 2181–2199 (1995). https://doi.org/10.1175/1520-0442(1995)008⟨2181:TMROTT⟩2.0.CO;2 .

[30] Held, I. M. & Soden, B. J. Robust Responses of the Hydrological Cycle to Global Warming. *Journal of Climate* **19** (21), 5686–5699 (2006). https://doi.org/10.1175/JCLI3990.1, publisher: American Meteorological Society Section: Journal of Climate .

[31] Jeevanjee, N. Three Rules for the Decrease of Tropical Convection With Global Warming. *Journal of Advances in Modeling Earth Systems* **14** (11), e2022MS003285 (2022). URL https://onlinelibrary.wiley.com/doi/abs/10.1029/2022MS003285. https://doi.org/10.1029/2022MS003285, _eprint: https://onlinelibrary.wiley.com/doi/pdf/10.1029/2022MS003285 .

[32] Singh, M. S., Kuang, Z., Maloney, E. D., Hannah, W. M. & Wolding, B. O. Increasing potential for intense tropical and subtropical thunderstorms under global warming. *Proceedings of the National Academy of Sciences* **114** (44), 11657–11662 (2017). https://doi.org/10.1073/pnas.1707603114 .

[33] Romps, D. M. Clausius–Clapeyron Scaling of CAPE from Analytical Solutions to RCE. *Journal of the Atmospheric Sciences* **73** (9), 3719–3737 (2016). https://doi.org/10.1175/JAS-D-15-0327.1, publisher: American Meteorological Society Section: Journal of the Atmospheric Sciences .

[34] Lilly, D. K. Cirrus outflow dynamics. *Journal of the Atmospheric Sciences* **45** (10), 1594–1605 (1988). https://doi.org/10.1175/1520-0469(1988)045⟨1594:COD⟩2.0.CO;2 .

[35] Jensen, E. J., van den Heever, S. C. & Grant, L. D. The Life Cycles of Ice Crystals Detrained From the Tops of Deep Convection. *Journal of Geophysical Research: Atmospheres* **123** (17), 9624–9634 (2018). https://doi.org/10.1029/2018JD028832, publisher: Blackwell Publishing Ltd .

[36] Schmidt, C. T. & Garrett, T. J. A Simple Framework for the Dynamic Response of Cirrus Clouds to Local Diabatic Radiative Heating. *Journal of the Atmospheric Sciences* **70** (5), 1409–1422 (2013). https://doi.org/10.1175/JAS-D-12-056.1 .

[37] Wall, C. J. *et al.* Observational Evidence that Radiative Heating Modifies the Life Cycle of Tropical Anvil Clouds. *Journal of Climate* **33** (20), 8621–8640 (2020). https://doi.org/10.1175/JCLI-D-20-0204.1 .

[38] Dobbie, S. & Jonas, P. Radiative influences on the structure and lifetime of cirrus clouds. *Quarterly Journal of the Royal Meteorological Society*

127 (578), 2663–2682 (2001). https://doi.org/10.1002/qj.49712757808, publisher: Wiley .

[39] Höjgård-Olsen, E., Chepfer, H. & Brogniez, H. Satellite Observed Sensitivity of Tropical Clouds and Moisture to Sea Surface Temperature on Various Time and Space Scales: 1. Focus on High Level Cloud Situations Over Ocean. *Journal of Geophysical Research: Atmospheres* **127** (6), e2021JD035438 (2022). https://doi.org/10.1029/2021JD035438 .

[40] Stubenrauch, C. J., Caria, G., Protopapadaki, S. E. & Hemmer, F. 3D radiative heating of tropical upper tropospheric cloud systems derived from synergistic A-Train observations and machine learning. *Atmospheric Chemistry and Physics* **21** (2), 1015–1034 (2021). https://doi.org/10.5194/acp-21-1015-2021 .

[41] Pierrehumbert, R. T. Thermostats, Radiator Fins, and the Local Runaway Greenhouse. *Journal of the Atmospheric Sciences* **52** (10), 1784–1806 (1995). https://doi.org/10.1175/1520-0469(1995)052⟨1784:TRFATL⟩2.0.CO;2 .

[42] Roe, G. H. & Baker, M. B. Why Is Climate Sensitivity So Unpredictable? *Science* **318** (5850), 629–632 (2007). URL https://www.science.org/doi/10.1126/science.1144735. https://doi.org/10.1126/science.1144735, publisher: American Association for the Advancement of Science .

[43] Wing, A. A. *et al.* Clouds and Convective Self-Aggregation in a Multi-Model Ensemble of Radiative-Convective Equilibrium Simulations. *Journal of Advances in Modeling Earth Systems* (2020). https://doi.org/10.1029/2020MS002138 .

[44] Stauffer, C. L. & Wing, A. A. Properties, Changes, and Controls of Deep-Convecting Clouds in Radiative-Convective Equilibrium. *Journal of Advances in Modeling Earth Systems* **14** (6), e2021MS002917 (2022). URL https://onlinelibrary.wiley.com/doi/abs/10.1029/2021MS002917. https://doi.org/10.1029/2021MS002917, _eprint: https://onlinelibrary.wiley.com/doi/pdf/10.1029/2021MS002917 .

[45] Hartmann, D. L. Tropical anvil clouds and climate sensitivity. *Proceedings of the National Academy of Sciences* **113** (32), 8897–8899 (2016). https://doi.org/10.1073/pnas.1610455113 .

[46] Gasparini, B. *et al.* Opinion: Tropical cirrus – from micro-scale processes to climate-scale impacts. *Atmospheric Chemistry and Physics* **23** (24), 15413–15444 (2023). https://doi.org/10.5194/acp-23-15413-2023 .

[47] Winker, D. M. *et al.* Overview of the CALIPSO Mission and CALIOP Data Processing Algorithms. *Journal of Atmospheric and*

Oceanic Technology **26** (11), 2310–2323 (2009). https://doi.org/10.1175/2009JTECHA1281.1 .

[48] Stephens, G. L. *et al.* The cloudsat mission and the A-Train: A new dimension of space-based observations of clouds and precipitation. *Bulletin of the American Meteorological Society* **83** (12), 1771–1790+1742 (2002). https://doi.org/10.1175/BAMS-83-12-1771 .

[49] Delanoë, J. & Hogan, R. J. Combined CloudSat-CALIPSO-MODIS retrievals of the properties of ice clouds. *Journal of Geophysical Research: Atmospheres* **115** (D4) (2010). https://doi.org/10.1029/2009JD012346 .

[50] Cazenave, Q. *et al.* Evolution of DARDAR-CLOUD ice cloud retrievals: New parameters and impacts on the retrieved microphysical properties. *Atmospheric Measurement Techniques* **12** (5), 2819–2835 (2019). https://doi.org/10.5194/amt-12-2819-2019 .

[51] Deng, M., Mace, G. G., Wang, Z. & Okamoto, H. Tropical Composition, Cloud and Climate Coupling Experiment validation for cirrus cloud profiling retrieval using CloudSat radar and CALIPSO lidar. *Journal of Geophysical Research: Atmospheres* **115** (D10) (2010). https://doi.org/10.1029/2009JD013104 .

[52] Sokol, A. B. & Hartmann, D. L. Congestus Mode Invigoration by Convective Aggregation in Simulations of Radiative-Convective Equilibrium. *Journal of Advances in Modeling Earth Systems* **14** (7) (2022). https://doi.org/10.1029/2022MS003045 .

[53] Khairoutdinov, M. F. & Randall, D. A. Cloud Resolving Modeling of the ARM Summer 1997 IOP: Model Formulation, Results, Uncertainties, and Sensitivities. *Journal of the Atmospheric Sciences* **60** (4), 607–625 (2003). https://doi.org/10.1175/1520-0469(2003)060⟨0607:CRMOTA⟩2.0.CO;2 .

[54] Morrison, H. *et al.* Parameterization of Cloud Microphysics Based on the Prediction of Bulk Ice Particle Properties. Part II: Case Study Comparisons with Observations and Other Schemes. *Journal of the Atmospheric Sciences* **72** (1), 312–339 (2015). https://doi.org/10.1175/JAS-D-14-0066.1 .

[55] Kang, H., Choi, Y.-S., Hwang, J. & Kim, H.-S. On the cloud radiative effect for tropical high clouds overlying low clouds. *Geoscience Letters* **7** (1), 7 (2020). https://doi.org/10.1186/s40562-020-00156-6 .

[56] Hong, Y., Liu, G. & Li, J.-L. F. Assessing the Radiative Effects of Global Ice Clouds Based on CloudSat and CALIPSO Measurements. *Journal of Climate* **29** (21), 7651–7674 (2016). https://doi.org/10.1175/JCLI-D-15-0799.1 .

[57] Kubar, T. L., Hartmann, D. L. & Wood, R. Radiative and Convective Driving of Tropical High Clouds. *Journal of Climate* **20** (22), 5510–5526 (2007). https://doi.org/10.1175/2007JCLI1628.1 .

[58] Cess, R. D. & Potter, G. L. A methodology for understanding and intercomparing atmospheric climate feedback processes in general circulation models. *Journal of Geophysical Research: Atmospheres* **93** (D7), 8305–8314 (1988). https://doi.org/10.1029/JD093iD07p08305 .

[59] Soden, B. J., Broccoli, A. J. & Hemler, R. S. On the Use of Cloud Forcing to Estimate Cloud Feedback. *Journal of Climate* **17** (19), 3661–3665 (2004). URL https://journals.ametsoc.org/view/journals/clim/17/19/1520-0442_2004_017_3661_otuocf_2.0.co_2.xml. https://doi.org/10.1175/1520-0442(2004)017⟨3661:OTUOCF⟩2.0.CO;2, publisher: American Meteorological Society Section: Journal of Climate .

[60] Lee, J.-Y. *et al.* in *Future Global Climate: Scenario-Based Projections and Near-Term Information* (eds V. Masson-Delmotte *et al.*) *Climate Change 2021: The Physical Science Basis. Contribution of Working Group I to the Sixth Assessment Report of the Intergovernmental Panel on Climate Chang* 553–672 (Cambridge University Press, Cambridge, United Kingdom and New York, NY, USA, 2021). Doi: 10.1017/9781009157896.006.